Solid-State NMR and X-ray Diffraction Study of Structure and Dynamics of Dihydrate and Anhydrous Form of Tyr-Ala-Phe

ARTICLE *in* CRYSTAL GROWTH & DESIGN · SEPTEMBER 2009

Impact Factor: 4.89 · DOI: 10.1021/cg900264x · Source: OAI

DOI: 10.1021/cg900264x

CRYSTAL GROWTH & DESIGN Article

2009, Vol. 9
4051–4059

Solid-State NMR and X-ray Diffraction Study of Structure and Dynamics of Dihydrate and Anhydrous Form of Tyr-Ala-Phe

Katarzyna Trzeciak-Karlikowska,[†] Anna Bujacz,[‡] Agata Jeziorna,[†] Włodzimierz Ciesielski,[†] Grzegorz D. Bujacz,[‡] Jarosław Gajda,[†] Danuta Pentak,[†,#] and Marek J. Potrzebowski*[,†]

[†]*Centre of Molecular and Macromolecular Studies, Polish Academy of Sciences, Sienkiewicza 112, 90-363 Lodz, Poland, and* [‡]*Institute of Technical Biochemistry, Technical University of Lodz, Stefanowskiego 4/10,90-924 Lodz, Poland.* [#]*On leave from University of Silesia, Institute of Chemistry, Department of Environmental Chemistry & Technology, Szkolna 9, PL-40006 Katowice, Poland.*

Received March 4, 2009; Revised Manuscript Received July 2, 2009

ABSTRACT: Tyr-D-Ala-Phe is a "message sequence" of naturally occurring opioid peptides, deltorphin I (Tyr-D-Ala-Phe-Asp-Val-Val-Gly-NH_2), deltorphin II (Tyr-D-Ala-Phe-Glu-Val-Val-Gly-NH_2), and dermorphin (Tyr-D-Ala-Phe-Gly-Tyr-Pro-Ser-NH_2). Analogous heptapeptides containing L-alanine instead of D-alanine are not biologically active. In a previous paper (*J. Phys. Chem. B* **2004**, *108* (14), 4535−4545), we reported X-ray and NMR data for Tyr-D-Ala-Phe. In the current report, we present structural studies of Tyr-Ala-Phe, a "false message sequence" of opioid peptides. It has been found that Tyr-Ala-Phe crystallizes in two forms, as anhydrate (Form I) and dihydrate (Form II). Crystal and molecular structure of both forms was established by means of low-temperature X-ray measurements. Form I is orthorhombic with space group $P2_12_12_1$, while II is hexagonal with space group $P6_5$. Solid-state NMR was employed to study the structure and molecular dynamics of I and II. Analysis of cross-polarization buildup curves and ^{13}C chemical shift tensor (CST) parameters obtained by a two-dimensional PASS experiment have revealed a dramatic difference in the molecular motion of both modifications. ^{13}C T_1 relaxation times have provided further evidence confirming distinct molecular dynamics. The attempt to understand the role of the stereochemistry of Ala residue in opioid peptide sequences in relation to intramolecular interactions and preorganization mechanisms is presented.

1. Introduction

Recent years have witnessed considerable interest in applications of opioid derivatives as promising pain controlling medicines.[1] Opioids have been used as analgesics for hundreds of years.[2] Drugs such as morphine and heroin are highly effective for controlling moderate and severe pain.[3] On the other hand the "side effects" related to abuse of and further addiction to opioids are known.[4] Hence one of the most challenging problems in deriving clinical benefits is to design better opioid drugs to eliminate or diminish these undesirable effects.

Opioid peptides (OPs) are a relatively new class of compounds with promising analgesic properties.[5] The enkephalins, the first endogenous opioid peptides, were isolated and identified from pig brain in 1975.[6] The second group of OPs, deltorphins and dermorphin, were extracted a little later from the skin of South American frogs.[7] The primary structure of the above-mentioned OPs is known. Enkephalins are pentapeptides consisting of Tyr-Gly-Gly-Phe-Leu (Lenk) or Tyr-Gly-Gly-Phe-Met (Menk). Deltorphin I (Tyr-D-Ala-Phe-Asp-Val-Val-Gly-NH_2), deltorphin II (Tyr-D-Ala-Phe-Glu-Val-Val-Gly-NH_2), and dermorphin (Tyr-D-Ala-Phe-Gly-Tyr-Pro-Ser-NH_2) are heptapeptides with identical first tripeptide sequences. The naturally occurring OP section containing two adjacent aromatic residues separated by one or two amino acids is responsible for the selectivity of receptor recognition. Schwyzer introduced the term "message domain" to refer to such a sequence.[8] In the cases of dermorphin and deltorphins, the message sequence consists of tyrosine, D-alanine, and phenylalanine. The presence of D amino acids is crucial for biological activity. It is interesting to note that heptapeptides consisting of L-alanine are not analgesics.[9] Hence, following Schwyzer's notation the Tyr-L-Ala-Phe sequence can be called a "false message domain".

The crucial point in understanding the biological activity of OPs is knowledge of the "bioactive shape" of the molecule and relative spatial positions of its aromatic rings. There are a number of experimental techniques and theoretical methods which allow investigation of structural restraints for biological samples.[10] Conformational studies for OPs performed by X-ray diffraction (XRD), solution NMR, solid state NMR, circular dichroism (CD), and fluorescence spectroscopy have been reported.[11] Deschamps recently exhaustively discussed the importance of crystallography in the structural analysis of opioids.[12] XRD provides unambiguous, accurate, and reliable three-dimensional structural data which are used for the analysis of spatial relationships. Solid-state NMR spectroscopy is a complementary technique to X-ray crystallography. A number of recently published papers have unambiguously proven that the term "NMR crystallography" is justified.[13]

In our previous paper, we reported a structural analysis of the Tyr-D-Ala-Phe message domain of dermorphin and deltorphins I and II employing X-ray and NMR.[14] We showed that both the stereochemistry of Ala residue and molecular packing can be factors determining the local molecular motion of Tyr-D-Ala-Phe and can be responsible for preorganization mechanisms. As concluded, the methyl residue of D-alanine can make the N-terminal part of the peptide rigid

*To whom correspondence should be addressed. Fax: +48 42 680 3261; tel: +48 42 680 3240; e-mail: marekpot@cbmm.lodz.pl.

Published on Web 08/04/2009

Scheme 1. Structure of Model Compounds with Carbon Atoms Labeled

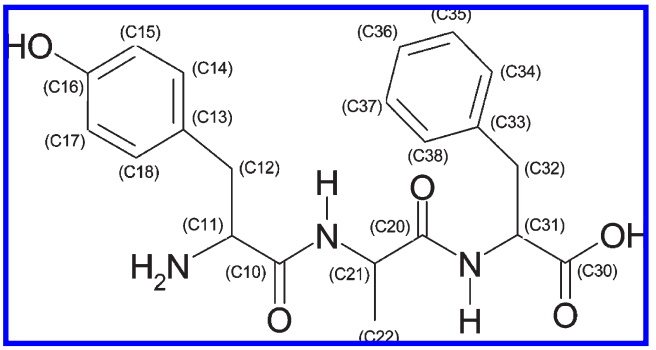

due to C−H···π interaction with only the phenyl group of tyrosine, strengthened by steric hindrance. We assumed that this effect is absent in the case of L-alanine tripeptide.

In the current work, we report on the structure and dynamics of Tyr-Ala-Phe tripeptides (Scheme 1). Having models with different stereochemistries we are in the position to answer the question of what is the influence of the chirality of Ala residue on chain conformations, crystal packing, and in consequence the molecular dynamics. Detailed X-ray analysis and solid state NMR data for Forms I and II of Tyr-L-Ala-Phe are reported.

2. Experimental Section

2.1. NMR Measurements. The solid-state cross-polarization magic angle spinning (CP MAS) ^{13}C NMR experiments were performed on a Bruker Avance III 300 spectrometer, at a frequency of 75.47 MHz, which was equipped with a MAS probe head using 4-mm ZrO_2 rotors. A sample of glycine (Gly) was used to set the Hartmann−Hahn condition and adamantane was used as a secondary chemical-shift reference at 38.48 and 29.46 ppm from external tetramethylsilane (TMS).[15] The conventional spectra were recorded with a proton 90° pulse length of 3.5 μs and a contact time of 1 ms. The repetition delay was 10 s and the spectral width was 25 kHz. Free induction decay (FID) spectra were accumulated with a time domain size of 2K data points. The ramped shape pulse was used during the cross-polarization (CP)[16] and two-pulse phase modulation (TPPM),[17] with tp = 6.8 ms and a phase angle of 20° during the acquisition. The CP efficiency was measured with contact times between 10 μs and 20 ms. The spectra data were processed using the WIN NMR program.[18] ^{13}C T_1 parameters in the solid state were measured at room temperature by means of a Torchia sequence.[19]

A sample spinning speed of 2 kHz was used in 2D-PASS experiments.[20] The 16-point $t1$ experiment data were replicated for 256 points. One-dimensional (1D) CSA spinning sidebands were obtained from $t1$ slices that were taken at isotropic chemical shifts in the two dimensions of the two-dimensional (2D) spectrum. The magnitudes of the principal elements of the chemical shift anisotropy (CSA) were obtained from the best fitting simulated spinning patterns. Simulations of the spinning CSA sidebands' spectra were performed on a personal computer (PC) using the SIMPSON program in a LINUX environment.[21]

2.2. X-ray Diffraction. The crystals of Form I, needle-shaped rods, were obtained by crystallization from water. Crystals were very thin and one species, with the dimensions 40 × 5 × 2 μm, was used for the diffraction experiment. Because of the small size of the crystal only a single run of data collection was performed with elongated exposure time for one image. Data were very weak and the Friedel pairs were merged during data processing. The axial reflections corresponding to two shorter cell dimensions were not visible in the data set, so the solution was performed in $P2_12_12_1$ and $P2_12_12$ space groups. The successful solution was obtained in $P2_12_12_1$. The full non-hydrogen atom model was obtained by the direct method. Hydrogen atoms connected to carbons were located geometrically and refined as riding. Hydrogen atoms connected to oxygen and nitrogen atoms were located on a difference Fourier map and refined with restrained distances. The temperature factors for all hydrogen atoms were assigned to be equal to 1.33 of the equivalent isotropic temperature factor of the parent atom. The data were collected on the X-13 beamline (EMBL, Hamburg, Germany) using a MAR CCD 165-mm detector, processed using DENZO, and scaled by SCALEPACK. All the observed reflections with $I > 0\sigma(I)$ were used to solve the structure by direct methods and refine it by full matrix least-squares using Fs.[22,23] Experimental details are presented in Table 1.

Table 1. Crystal Data and Experimental Details of Tyr(L)AlaPhe

	Crystal Form I	Crystal Form II
molecular formula	$C_{21}H_{25}N_3O_5$	$C_{21}H_{25}N_3O_5 \cdot H_20$
formula weight	399.44	417.46
crystallographic system	orthorhombic	hexagonal
space group	$P2_12_12$	$P6_5$
a (Å)	8.653(2)	11.946(2)
b (Å)	39.737(8)	11.946(2)
c (Å)	5.523(1)	54.991(11)
α (°), β (°), γ (°)	90, 90, 90	90, 90, 120
V (Å^3)	1899.1(7)	6796.2(19)
Z	4	12
D_c (g/cm^3)	1.397	1.224
μ [cm^{-1}]	1.01	0.90
Measurement Details		
crystal dimensions [μm]	40 × 5 × 2	80 × 80 × 10
wavelength [Å]	0.8010	0.8162
maximum 2θ (°)	52.72	65,93
T_{meas} (K)	100	100
Data Processing		
resolution [Å]	40−0.90 (0.93−0.90)	60.0−0.75 (0.78−0.75)
R_{merge} [%]	12.9 (68.6)	4.8 (8.5)
completeness [%]	85.7 (82.0)	99.5 (98.6)
no. of reflections	5230	251351
no of unique reflections	1429	5719
redundancy	3.7 (3.6)	25.8 (13.3)
$I/\sigma < I >$	10.72 (1.87)	83.33 (31.76)
Refinement Statistics		
no. of reflections: unique	1429	11267
with $I > 0\sigma(I)$	1410	11188
obs. with $I > 2\sigma(I)$	1030	11153
no. of parameters refined	266	630
R_{obs}	0.0668	0.0616
wR_{obs}	0.1554	0.1537
S_{obs}	1.004	1.075

The crystals of Form II were obtained from a methanol−water mixture. After cooling of the mixture, small hexagonal plates appeared in the solution. The monocrystal, which had dimensions of 50 × 50 × 10 μm, was removed from the solution and mounted on the MicroMounts loop using a thin layer of oil. Two runs, corresponding to high and low resolution, were performed. The exposition time for the low resolution run was 10 times shorter than for the high run to avoid overload reflections. The structure was solved for both enantiomorphic space groups: $P6_1$ and $P6_5$. Although models were obtained for both of them, the model for $P6_5$ was used because of a wrong chirality in $P6_1$. During refinement a partial merohedral twinning was identified and a fraction of the twinning was implemented into the refinement. The fraction of the unit cells with reverse orientation (010 100 00$\bar{1}$) was refined as 0.2641. A number of crystals of II from different crystallizations were measured, and all were found to be merohedral twins. The hydrogen atoms were located and refined to the orthorhombic crystal form. Anisotropic thermal parameters were refined for all non-hydrogen atoms. Two alternative positions were identified for both water molecules presented in the asymmetric unit. The occupation factors for these two water molecules were refined as complementary to one. Usage of synchrotron radiation for structural analysis allowed us to obtain a

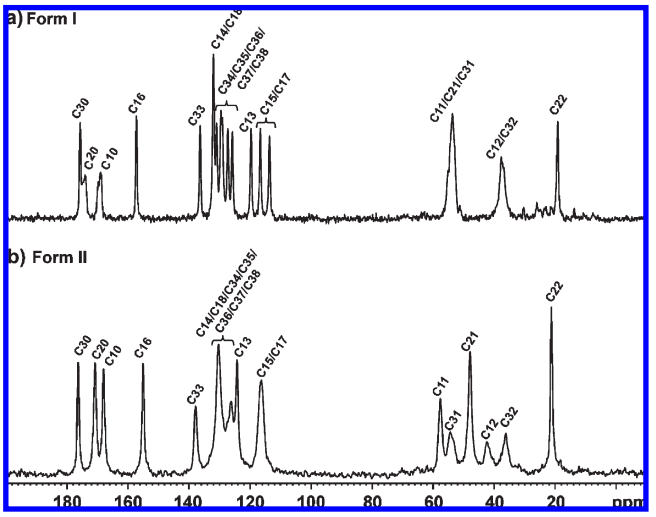

Figure 1. ^{13}C CP/MAS spectra of two forms of Tyr-Ala-Phe: (a) crystallized from water; (b) crystallized from a water−methanol mixture. The assignment of ^{13}C resonances is shown.

crystal structure for an extremely small monocrystal and for twinned with better statistical parameters in comparison to data obtained by standard diffractometers. Crystal data were deposited in the Cambridge Crystallographic Data Centre under CCDC 720512 and CCDC 720511 (Form I and Form II, respectively).

3. Results and Discussion

3.1. ^{13}C NMR Study of Tyr-L-Ala-Phe 1. ^{13}C CP/MAS spectra of **1** recorded at 8 kHz spinning rate are shown in Figure 1. From comparison of spectra, it is clear that **1** exists in at least two forms. Figure 1a displays the ^{13}C CP/MAS spectrum of the sample crystallized from water (Form I). The resonance lines are very sharp and their assignment is straightforward. The line-shape analysis of carbonyl groups Tyr10 and Ala20 shows splitting. The origin of asymmetric splitting of ^{13}C resonances induced by ^{14}N nuclei in the solid state was discussed in detail by Diaz and co-workers.[24] $^{13}C-^{14}N$ residual dipolar coupling is observed because ^{14}N eigenstates are not pure Zeeman states but are determined by the Zeeman-quadrupole Hamiltonian. MAS is not able to average this coupling to zero, leading to both splitting and broadening of ^{13}C signals.

Aromatic signals are very well resolved. The three aliphatic CH signals (Figure 1a) are overlapped and are observed as a broadened line at $\delta = 53.6$ ppm. A similar observation is made regarding two CH_2 signals coming from Tyr and Phe residues. They are found at $\delta = 37.6$ ppm. The signal representing the methyl group of alanine is at $\delta = 21.3$ ppm.

Figure 1b displays the ^{13}C CP/MAS spectrum of sample crystallized from a methanol−water mixture (vol/vol 1:1) (Form II). From comparative analysis of spectra, it is apparent that both forms differ significantly in their molecular packing. Each region (carboxyl/carbonyl, aromatic, and aliphatic) looks different. The $^{13}C-^{14}N$ splitting is not seen for C10 and C20 carbonyls. Resolution of signals for aromatic residues of tyrosine and phenylalanine is not as good as for Form I. It is worth noting that in the region of 113−120 ppm, instead of three signals we observe only one at $\delta = 116.7$ ppm. On the other hand, the aliphatic signals of methylene (Phe 32, Tyr 12) and methine carbons (Phe 31 and Tyr 11) are much better separated for II than for I. The broadening and splitting of signals for II is because two inequivalent molecules of TyrAlaPhe are in the asymmetric unit.

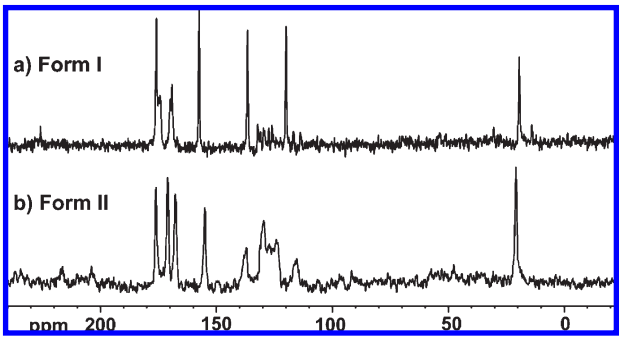

Figure 2. Dipolar dephasing (DD) spectra of two Forms of Tyr-L-Ala-Phe. Spectra were recorded with dipolar delay equal to 55 μs.

Figure 2 shows ^{13}C NMR spectra obtained using a dipolar dephasing (DD) pulse sequence.[25] This method is often used as a spectral editing technique. In the simplest approach after CP, the ^{1}H decoupler is turned off for ca. 55 μs. This is sufficient time for $^{13}C-^{1}H$ dipolar coupling to dephase the transverse magnetization of any ^{13}C isotope with a directly bonded ^{1}H isotope, as long as the dipolar coupling is not motionally averaged. In the case of Form I, the lines for rigid CH and CH_2 are effectively suppressed while quaternary signals are observed. The methyl group is under a fast exchange regime and its signal is only attenuated. Interesting information is provided by an analysis of the spectrum shown in Figure 2b, which was recorded under exactly the same conditions as for Figure 2a. As seen, for a dipolar delay equal to 55 μs, aromatic signals are not suppressed. According to a statement given supra we can assume that phenyl rings are under a fast exchange regime. Thus we can conclude that I and II differ not only in molecular packing but also in molecular dynamics. Unfortunately the DD experiment does not give a clear answer as to which aromatic group (Phe, Tyr, or both) is under the fast exchange regime.

3.2. Molecular Dynamics of Forms I and II of Tyr-Ala-Phe: Measurement of Relaxation Times. SSNMR is an analytical technique that systematically extends the repertoire of novel approaches, allowing a better understanding of the nature of the condensed matter. This field was recently exhaustively reviewed, and a number of papers have been published.[26] Significant contributions regarding SSNMR studies of organic compounds and pharmaceuticals have been made by Harris' group.[27] A number of systems were investigated by employing mostly 1D high-resolution NMR. Isotropic chemical shifts, chemical shift tensor (CST) parameters, and measurements of relaxation times have been reported for several systems. Such parameters as ^{13}C and ^{1}H spin−lattice relaxation times (^{13}C T_1 and ^{1}H T_1), carbon and proton rotating frame relaxation times (^{13}C $T_{1\rho}$ and ^{1}H $T_{1\rho}$), the C−H cross-relaxation constant (T_{C-H}), and the proton relaxation time in the dipolar state (T_{1D})[28] exhibit substantial utility for elucidating the dynamics of forms. Not all of these parameters provide direct information, but under favorable circumstances it is possible to establish amplitudes and motional frequencies for solids in a broad range.

As we found, an analysis of the CP profiles[29] constitutes an important source of information concerning the molecular dynamics of I and II (Figure 3).

$$I(t) = I_0(1 - T_{IS}/T_1\rho H)^{-1}[\exp(-t/T_1\rho H) - \exp(-t/T_{IS})] \quad (1)$$

In CP eq 1 for the IS model, the first time constant T_{IS} characterizes the increase in the polarization transfer, which is

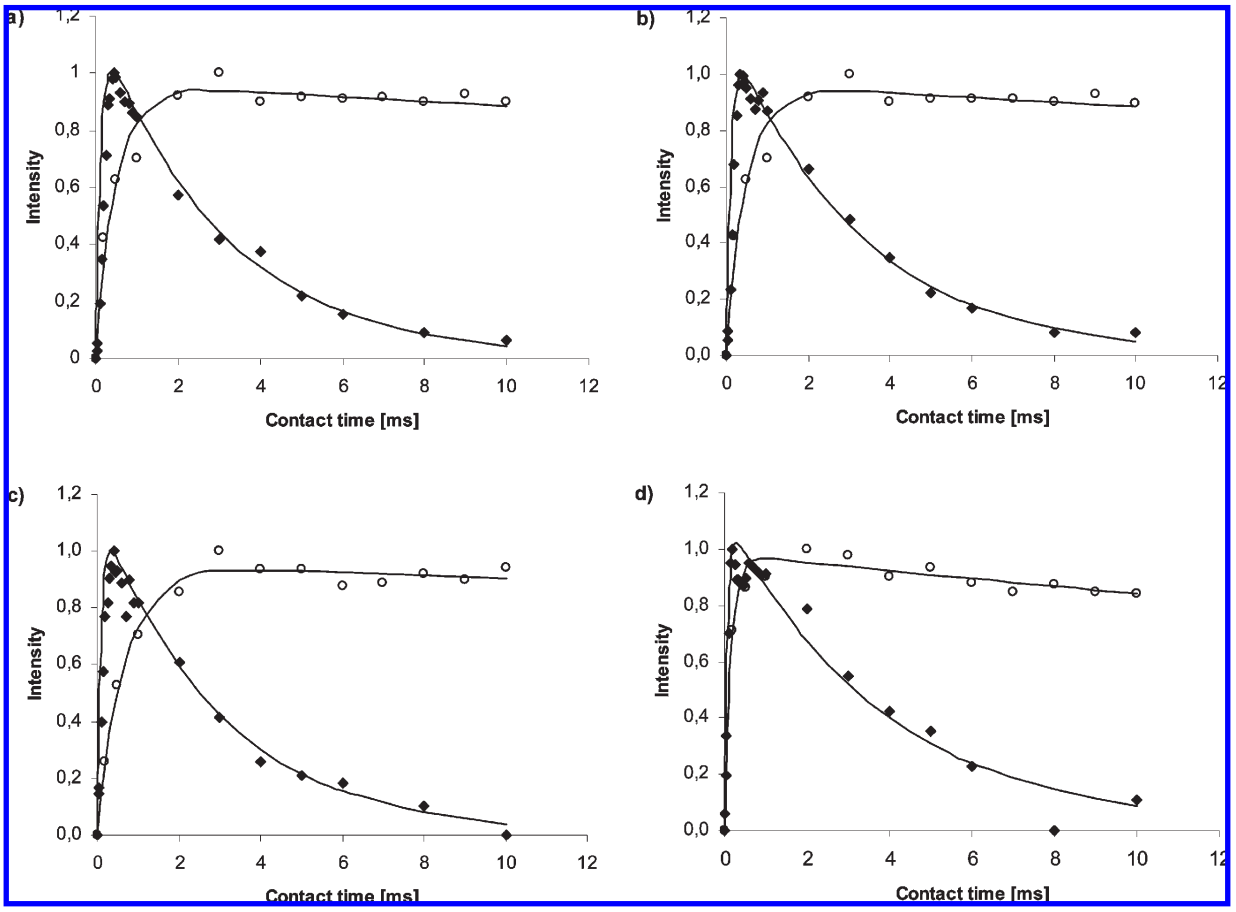

Figure 3. Cross-polarization (CP) as a function of contact time for the (a) C30, (b) C10, (c) C33, and (d) C22 carbons; the data points represent the experimental data and the solid lines correspond to the fitted curve (○: Form I; ♦: Form II) using eq 1.

Table 2. Dynamic Parameters ^{1}H $T_{1\rho}$ and ^{13}C T_1 for Form I and Form II in the Solid Phase

form I					form II				
carbon no.	δ_{iso} [ppm]	T_{IS} [ms]	$T_{1\rho}$ [ms]	T_1 [s]	carbon no.	δ_{iso} [ppm]	T_{IS} [ms]	$T_{1\rho}$ [ms]	T_1 [s]
30	175	0.66	91.55	106.4	30	176	0.12	3.03	7.65
20	173	0.96	112.14	70.9	20	171	0.11	3.50	12.33
10	168	1.02	85.79	87.7	10	168	0.12	3.20	16.29
16	156	0.88	125.58	158.7	16	155	0.08	3.50	7.72
33	135	0.68	162.12	102.0	33	137	0.09	2.98	12.30
14/18	130	0.36	89.83	108.7	14/18/ 34/35/36/ 37/38	130	0.02	2.45	3.68
34/35/ 36/37/38	128	0.26	80.11	116.3					
	126	0.38	68.55	83.3	15/17	125	0.08	3.30	5.03
	125	0.46	74.18	69.90	13	116	0.08	2.78	2.62
13	119	0.70	183.05	113.6	11/31	55	0.06	3.20	5.51
15/17	115	0.35	92.51	142.9	21	48	0.23	3.60	7.20
	113	0.30	98.28	151.5	12	42	0.02	2.60	6.46
11/21/31	52	0.16	72.57	33.4	32	36	0.02	2.60	10.91
12/32	36	0.12	76.08	90.1	22	21	0.07	3.90	0.34
22	18	0.26	65.12						

dependent on the inverse direct C−H dipole−dipole interaction (leading to a steep increase in ^{13}C polarization at starting contact times). The second time constant characterizes the decrease in magnetization: $T_{1\rho H}$, which is the relaxation time of the protons in the rotating frame. Figure 3 shows selected CP buildup curves of both forms (C30 carboxyls, C10 carbonyls, C33 aromatic, and C22 aliphatic signals). From analysis of the profiles of I and II, the dramatic distinction of CP parameters is apparent. The T_{IS} constant and $T_{1\rho H}$ relaxation time for all carbons of Forms I and II are presented in Table 2. For Form I the $T_{1\rho H}$ for all carbons are in the range 60−200 ms, while for Form II they are in the range 2.5−4 ms. We assume that the discrepancy in relaxation parameters is due to differences in molecular packing. For Form I, molecules of I in the crystallographic unit are very tightly packed with limited space for molecular motion, while for sample II the density is low and large amplitude molecular motion of side chains of peptide is allowed. The T_{IS} constants for Form I are a few times larger compared to II. This phenomenon is related to molecular motion. As proven by Fulber et al., the CP constants are sensitive to the slow motions which modulate both heteronuclear and homonuclear dipolar interactions.[30]

Further proofs confirming the distinct molecular motion of I and II were taken from measurements of ^{13}C T_1 relaxation

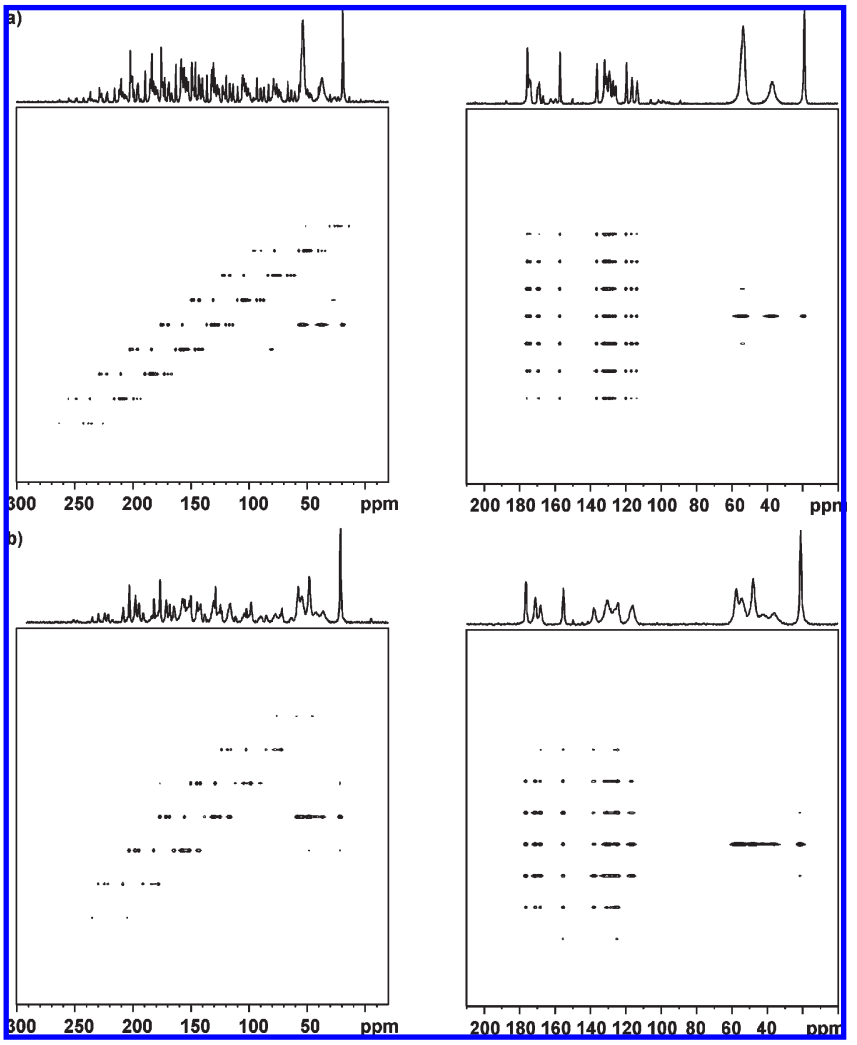

Figure 4. 2D PASS spectra of (a) Form I and (b) Form II recorded with a spinning rate of 2 kHz (left) and after data shearing (right).

times employing the pulse sequence published elsewhere.[19] The T_1 relaxation parameters for both forms are presented in Table 2. As one can see, ^{13}C T_1 for I are very long while for II they are several times shorter. The dramatic distinction is seen for CH aromatic carbons (which are almost 20 times longer for I). Short ^{13}C T_1 relaxation times for Tyr and Phe CH carbons of II suggest that both aromatic groups are under fast exchange regimes.

3.3. Comparative Analysis of ^{13}C δ_{ii} Chemical Shift Tensor (CST) Parameters. Detailed information was obtained about the electronic surroundings of each nucleus, which reflect subtle structural effects. For example, hydrogen bonding and internal molecular motion can be obtained from inspection of the tensorial nature of the chemical shift. Hence, we were attracted by the prospect of analysis of ^{13}C δ_{ii} data, inspection of anisotropic values of CSTs, and correlation of the principal elements to the molecular structure for both forms.

For rotating solids, ^{13}C δ_{ii} (ii = 11, 22, 33) parameters can be obtained from the analysis of spinning sideband intensities. For the sample under investigation, a spinning rate in the range of 2−3 kHz is required to obtain the spectrum with a sufficient number of sidebands for further calculations of the aromatic and carboxyl/carbonyl regions. In the current work, we have not analyzed the ^{13}C CST parameters of aliphatic carbons.

There are several approaches that allow separation of the isotropic and anisotropic parts of spectra with heavy overlapped systems.[31] In our project, we employed the 2D PASS sequence, which offers good sensitivity compared to other techniques and does not require any hardware modifications or special probehead.

Figure 4 displays the 2D PASS spectra for Forms I and II recorded at the spinning rate of 2 kHz. The carbonyl group and aromatic atoms are characterized by large CSA, and under slow sample spinning the spectra present a complex pattern. By proper data shearing (Figure 4a, right, and b, right) it is possible to separate the spinning sidebands for each carbon and to employ a calculation procedure to establish the ^{13}C δ_{ii} parameters. It is clear from such a presentation that the F2 projection corresponds to the TOSS[32] spectrum while F1 represents CSA.

The ^{13}C δ_{ii} values (Table 3) were obtained by means of the SIMPSON program.[21] The experimental (left column) and the best-fitting simulated 1D spinning CSA sideband patterns (middle column) for selected carbons are shown in Figure 5. The upper traces represent Form I and the bottom traces Form II. In order to better visualize in pictorial form the distinction between ^{13}C CST parameters we also present simulated static line-shapes (right column).

^{13}C δ_{ii} elements for carboxyl group (C30) are typical of the deprotonated, zwitterionic form of amino acids.[33,34] For

Table 3. Values of the ^{13}C Isotropic (δ_{iso}) and Calculated Chemical Shift Parameters (δ_{ii}) and Corresponding Anisotropic Parameters[a] of Forms I and II

form I							form II						
carbon no.	δ_{iso} [ppm]	δ_{11} [ppm]	δ_{22} [ppm]	δ_{33} [ppm]	Ω [ppm]	κ [ppm]	carbon no.	δ_{iso} [ppm]	δ_{11} [ppm]	δ_{22} [ppm]	δ_{33} [ppm]	Ω [ppm]	κ [ppm]
30	175.7	247	168	111	136	−0.17	30	176.4	237	186	107	130	0.21
20	174.8	239	193	91	148	0.38	20	171.1	244	179	91	153	0.15
10	169.3	252	167	90	162	−0.05	10	168.1	245	169	90	156	0.02
16	157.2	241	163	67	174	0.10	16	155.2	245	144	77	168	−0.19
33	136.3	234	163	11	223	0.36	33	138.0	224	164	26	197	0.39
14/18	131.9	225	143	28	197	0.17	14/18/ 34/35/ 36/ 37/38	130.5	183	156	52	131	0.59
34/ 35/	130.9	222	143	27	195	0.19	13	124.5	219	126	29	190	0.02
36/37/ 38	129.3	224	145	18	206	0.23	15/17	115.9	149	149	49	100	1.00
	127.2	224	142	15	209	0.21							
	125.7	218	146	13	205	0.30							
13	119.6	213	134	12	201	0.21							
15/17	116.6	189	134	27	162	0.32							
	113.6	189	126	26	163	0.23							

[a] The ^{13}C δ_{ii} parameters are defined as follows: $\delta_{11} \geq \delta_{22} \geq \delta_{33}$. The estimated error in δ_{11}, δ_{22}, and δ_{33} is ± 3 ppm; $\delta_{iso} = (\delta_{11} + \delta_{22} + \delta_{33})/3$, span is expressed as $\Omega = \delta_{11} - \delta_{33}$, and skew is expressed as $\kappa = 3(\delta_{22} - \delta_{iso})/\Omega$.

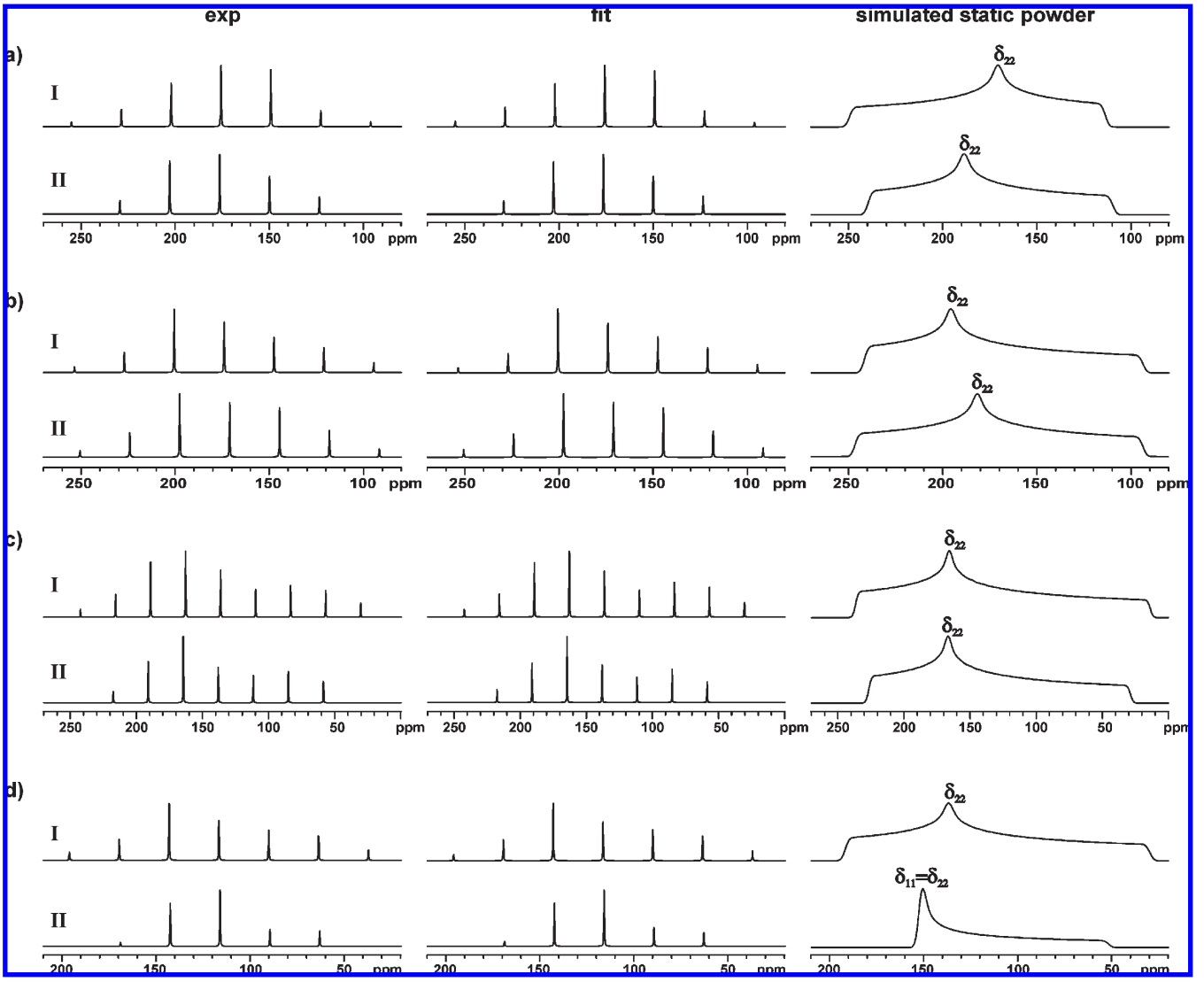

Figure 5. Experimental and best-fitting simulated 1D spinning CSA sideband patterns of Forms I and II for (a) C30, (b) C20, (c) C33, and (d) C15/17. The ^{13}C tensor for C15/C17 carbons of Form II is axially symmetric.

both forms the Ω is very similar and very close to the value established for Tyr-D-Ala-Phe. The larger value of ^{13}C δ_{22} for II (a bottom trace of 5a) compared to I suggests that the former form contributes to stronger hydrogen bonding as donor. The CST values of peptide carbons (C10 and C20) require a short comment. For Form II, ^{13}C δ_{iso} values differ

Scheme 2. Orientation of the ^{13}C Principal Elements of the Chemical Shift Tensor (CST) Components with Respect to the Bond Geometry

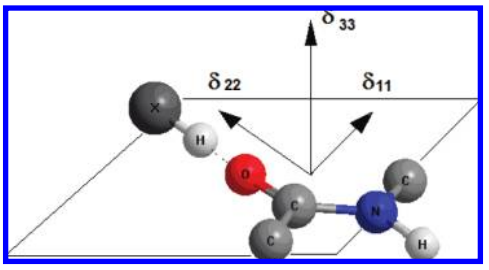

by ca. 3 ppm. ^{13}C δ_{33} are similar while ^{13}C δ_{22} differ by 10 ppm. Ando and co-workers have reported linear correlation between ^{13}C δ_{ii} parameters and the strength of the >C=O···H−N< hydrogen bonding.[35] The orientation of the ^{13}C principal elements of CST with respect to the molecular frame of amide carbonyl carbon is shown in Scheme 2.

The δ_{11} is in the amide sp^2 plane and lies along a direction normal to the C=O bond, the δ_{22} component lies almost along the amide C=O bond, and the δ_{33} component is aligned perpendicular to the amide sp^2 plane. It is apparent that the most sensitive parameter which best reflects the nature of hydrogen bonding is δ_{22}. The values of δ_{22} components established for amide carbons of II are 179 and 169 ppm for C(20)=O and C(10)=O, respectively.[36] For Form I, the values of δ_{22} components established for amide carbons are 193 (upper trace of 5b) and 167 ppm. The difference of 26 ppm suggests a significant distinction in the strength of the hydrogen bonding.

The ^{13}C δ_{ii} values completed in our project were compared with data for corresponding aromatic amino acids reported by Ye at al.[37] From analysis of data for both forms, it is apparent that values of ^{13}C δ_{ii} elements of aromatic CH carbons are dramatically different (Figure 5d). This conclusion is valid for phenyl rings of both amino acids (Tyr, Phe). For instance, the span parameter Ω for carbons C15/C17 (Tyr) is found to be 163 ppm for Form I and 100 ppm for Form II (bottom trace 6d). A similar distinction is seen for phenylalanine CH carbons (Ω is equal to 207 ppm for Form I and 130 ppm for Form II). The differences between Ω of aromatic quaternary carbons (Figure 5c) are not so spectacular (in the range of a few ppm). These results clearly prove that the phenyl rings of forms are under very different dynamic regimes. The chemical shift anisotropy for Form II is reduced due to the fast molecular motion, which is very likely around the 1−4 axis of the ring.

3.4. X-ray Crystal Structures of Form I and Form II. Measurements of Forms I and II were carried out on a synchrotron at 100 K (see Experimental Section). The crystals of Form I crystallized in the orthorhombic $P2_12_12_1$ space group with the asymmetric unit containing a single peptide molecule. The molecules in the crystal lattice are tightly packed, and the crystal density is much bigger than in Form II (see Table 1). The peptide molecule has zwitterionic form, with a protonated, positively charged N-terminal group and deprotonated, negatively charged C-terminal group. The molecule has a twisted conformation with the carboxyl, ammonia, and hydroxyl groups located on one side of the molecule and hydrophobic side chains of alanine and phenylalanine on the other side of the molecule (Figure 6a).

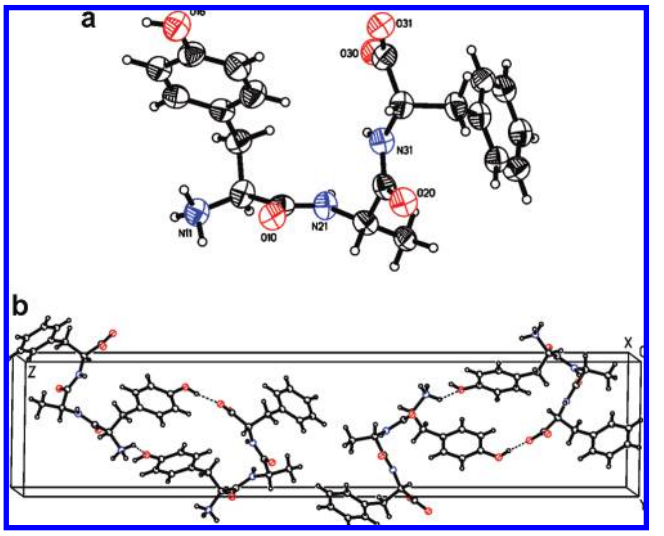

Figure 6. The crystal structure of Form I, (a) ORTEP plot of one peptide molecule with numbered heteroatoms, (b) the crystal packing of the unit cell.

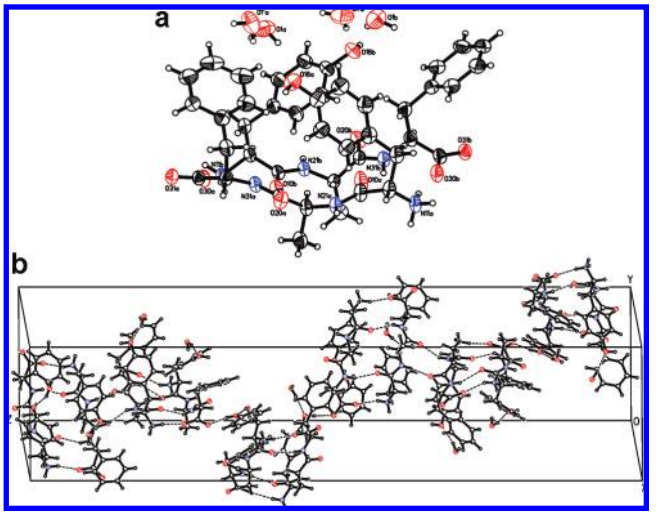

Figure 7. The crystal structure of Form II. (a) The ORTEP plot of the dimer and two water molecules creating independent unit (disordered waters with lower occupancy are shown with dotted line), (b) the crystal packing of the unit cell.

The packing of molecules in the unit cell is shown in Figure 6b. This peptide molecule does not possess any intramolecular hydrogen bonds. In this form the most eye-catching elements are the chains of molecules related by a 100 translation. These chains are formed by strong hydrogen bonds between the protonated amino group and the deprotonated carboxyl group of the translated molecule. Along the chains, the methyl groups are located between phenyl rings and create two weak CH···π interactions. These chains are linked together with the next chain related by a 001 translation. The interactions responsible for this connection are hydrogen bonds between the other hydrogen from the ammonia group and the carboxylic group of the symmetry-related molecule and also the hydrogen bond between the peptide hydrogen of alanine and the peptide oxygen of the next (001 translated) alanine. The linked chains form layers of molecules located in the *xz* plane (010 planes). These layers of molecules have two surfaces: the hydrophilic one is

Table 4. Selected Hydrogen-Bonding Geometry for Forms I and II of Tyr-L-Ala-Phe

form I					form II				
D−H···A	D−H (Å)	H···A (Å)	D···A (Å)	D−H···A (deg.)	D−H···A/B	D−H (Å)	H···A/ (Å)	D···A/ B (Å)	D−H···A/ B (deg.)
N11−H···O30	0.950	1.810	2.723	160.32	$N11_A$−H···$O30_A$	0.889	1.903	2.776	166.78
N11−H···O31	0.951	1.891	2.789	156.60	$N11_A$−H···$O30_B$	0.887	1.967	2.831	164.24
N11−H···O16	0.950	2.207	2.916	130.56	$O16_A$−H···$O31_B$	0.850	1.806	2.639	166.61
O16−H···O31	0.849	1.741	2.583	170.98	$N21_A$−H···$O20_B$	0.860	2.095	2.884	152.28
N21−H···O20	0.900	1.811	2.704	171.65	$N11_B$−H···$O30_B$	0.889	2.126	2.941	172.72
					$N11_B$−H···$O30_A$	0.892	2.126	2.947	152.47
					$O16_B$−H···$O31_A$	0.851	1.741	2.589	174.45
					$N21_B$−H···$O20_A$	0.860	2.119	2.855	143.28
					$N31_B$−H···$O10_A$	0.861	2.117	2.833	140.29

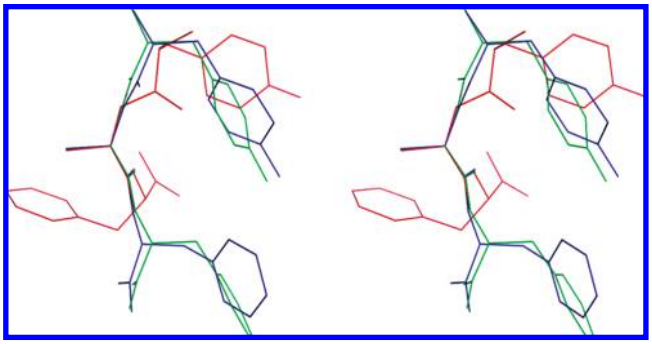

Figure 8. The stereodiagram of the aligned molecules from both forms based on the superposition of the central alanine residue (red color − Form I, blue and green − Form II).

created by ammonia and carboxyl groups and hydroxyl of the tyrosine side chain; the second surface has a hydrophobic character and is created by phenylalanine and alanine side chains. Every second layer has reverse orientation and interacts by hydrophobic and hydrophilic interfaces. Two main interactions of the hydrophilic interface involve hydrogen bonds created by the hydroxyl tyrosine group.

The hydrogen from this group creates a hydrogen bond with the carboxyl oxygen from the next layer and at the same time hydroxyl oxygen serves as an acceptor for hydrogen of the ammonia group. Selected hydrogen bond parameters are presented in Table 4. The main interactions of the hydrophobic interface are the van der Waals contacts between the phenyl ring of phenylalanine and the methyl group of alanine. These interactions create a zipper-like structure. The bulky phenyl ring is located on the opposite side of the small methyl group.

The crystals of Form II are hexagonal with space group $P6_5$. The peptide dimer and two water molecules create the independent unit (Figure 7a). The crystal packing of molecules in the unit cell of Form II is shown in Figure 7b. The unit cell has large dimension, and consists of 12 molecules, with two peptide molecules and two water molecules in the asymmetric unit. Both independent peptide molecules exist in zwitterionic form with positively charged terminal amine groups and deprotonated carboxylic groups. These two molecules create a "head to tail" type of dimer. The four strong hydrogen bonds (Table 4) are responsible for the dimer formation, the architecture of which resembles a short antiparallel β-sheet. The network of hydrogen bonds occurs between the carboxyl group of Phe and the amine group of Tyr and between the peptide hydrogen of Phe and the carboxyl oxygen of Tyr. Because the dimer has a pseudo, 2-fold axis, these two hydrogen bonds are repeated by symmetry-related groups. The peptide's hydrogens and carbonyl oxygens of the central Ala in both molecules are not involved in dimer formation, but they are responsible for interactions with the next dimer related by the 6-fold screw axis. In addition to the helical arrangements of the dimers along the 6-fold axis, chains of dimers perpendicular to this axis can be observed. These perpendicular chains are stabilized by hydrogen bonds between the N-terminal amine group and the C-terminal carboxyl group of the same monomer from the molecule related by translation. Analogous chains, created by other monomers from the dimers, run in parallel but in the opposite direction. Water molecules are trapped in the cage created by Phe and Tyr side chains and terminal amine and the carboxyl groups from symmetry-related molecules. Their position is maintained by the hydrogen bonds created between them, the hydroxyl group of Tyr, and the terminal amine group of Tyr from the symmetry-related molecule. The methyl groups from the Ala residues create hydrophobic van der Waals contacts with the phenyl rings of the Phe from the symmetry-related molecule, but they do not create a C−H···π hydrogen bond, in contrast to the previously described crystal structure of Tyr-D-Ala-Phe.[14] The conformation of both molecules creating a dimer in Form II is different than the molecule in Form I. The conformation of the molecule in Form I reassembles to α helix and in Form II remains β sheet. The differences in molecules conformations in both forms are very visible after superposing of the central alanine (Figure 8).

4. Conclusions

Results shown in this work for Tyr-L-Ala-Phe and comparative analysis with Tyr-D-Ala-Phe published elsewhere[14] shed new light on the role of D-alanine in the message sequence of opioid peptides. As mentioned supra, "bioactive conformation" appears to be one of the crucial features responsible for specificity and in consequence for the selectivity of ligand action. Our X-ray and NMR studies prove that Tyr-L-Ala-Phe forms conformational modifications very easily. It means that this system is very flexible. In our previous paper we revealed that C−H···π interaction between the methyl group of D-alanine and the phenyl ring of tyrosine is one of the important structural constraints which makes the "message sequence" relatively rigid. This effect can be important in the preorganization mechanism during crystal growth and very likely during peptide−receptor interaction.

Acknowledgment. The authors are grateful to the State Committee for Scientific Research (MIiN) for financial support, Grant No. N N204 1313 35.

References

(1) (a) Donnelly, S.; Davis, M. P.; Walsh, D.; Naughton, M. *Supp. Care Cancer* 2002, *10*, 13−35, and references cited therein; (b) Przewłocki, R.; Przewłocka, B. *Eur. J. Pharmacol.* **2001**, *429*, 79–91.

(2) Browstein, M. J. *Proc. Natl. Acad. Sci. U.S.A.* **1993**, *90*, 5391–5393.
(3) Kalso, E. *Eur. J. Pain* 2005, *9*, 131−135 and references cited therein.
(4) Miller, R. J.; Tran, P. B. *Trends Pharmacol. Sci.* **2000**, *21*, 299–304.
(5) Thematic Issue, *Curr. Top. Med. Chem.* 2004, *4*, 1−157.
(6) Hughes, J.; Smith, T. W.; Kosterlitz, H. W.; Fothergill, L. A.; Morgan, B. A.; Morris, H. R. *Nature* **1975**, *258*, 577–579.
(7) Erspamer, V. *Int. J. Dev. Neurosci.* **1992**, *10*, 3–30.
(8) Schwyzer, R. *Biochemistry* **1986**, *25*, 6335–6342.
(9) Jilek, A.; Kreil, G. *Monatsh. Chem.* 2008, *139*, 1−5 and references cited therein.
(10) Schermann, J. P. In *Spectroscopy and Modeling of Biomolecular Building Blocks*; Elsevier Science: Amsterdam, 2007; pp 1−480.
(11) (a) Naito, A.; Nishimura, K. *Curr. Top. Med. Chem.* **2004**, *4*, 135–145. (b) Dhanasekaran, M.; Palian, M. M.; Alves, I.; Yeomans, L.; Keyari, C. M.; Davis, P.; Bilsky, E. J.; Egleton, R. D.; Yamamura, H. I.; Jacobsen, N. E.; Tollin, G.; Hruby, V. J.; Porreca, F.; Polt, R. *J. Am. Chem. Soc.* **2005**, *127*, 5435–5448. (c) Podlogar, B. L.; Paterlini, M. G.; Ferguson, D. M.; Leo, G. C.; Demeter, D. A.; Brown, F. K.; Reitz, A. B. *FEBS Lett.* **1998**, *439*, 13–20.
(12) Deschamps, J. R. *AAPS J.* **2005**, *7*, E813–E819.
(13) (a) Brouwer, D. H. *J. Magn. Reson.* **2008**, *194*, 136–146. (b) Brouwer, D. H. *J. Am. Chem. Soc.* **2008**, *130*, 6306–6307. (c) Harris, R. K.; Hodgkinson, P.; Pickard, C. J.; Yates, J. R.; Zorin, V. *Magn. Reson. Chem.* **2007**, *45*, S174–S186. (d) Varga, K.; Ashmovska, L.; Parrot, I.; Dauvergne, M. T.; Haertlein, M.; Forsyth, V.; Watts, A. *Biochim. Biophys. Acta − Biomembr.* **2007**, *1768*, 3029–3035. (e) Harris, R. K. *Solid State Sci.* **2004**, *6*, 1025–1037. (f) Taulelle, F. *Solid State Sci.* **2004**, *6*, 1053–1057.
(14) Slabicki, M. M.; Potrzebowski, M. J.; Bujacz, G.; Olejniczak, S.; Olczak, J. *J. Phys. Chem. B* **2004**, *108*, 4535–4545.
(15) Morcombe, C. R.; Zilm, K. W. *J. Magn. Reson.* **2003**, *162*, 479–486.
(16) Metz, G.; Wu, X.; Smith, S. O. *J. Magn. Reson. Ser. A* **1994**, *110*, 219–227.
(17) Bennett, A. W.; Rienstra, C. M.; Auger, M.; Lakshmi, K. V.; Griffin, R. G. *J. Chem. Phys.* **1995**, *103*, 6951–6957.
(18) *Win-NMR, Bruker−Franzen Analytik GmbH*, version 6.0; Bremen, Germany, 1993.
(19) Torchia, D. A. *J. Magn. Reson.* **1978**, *30*, 613–616.
(20) (a) Antzutkin, O. N.; Shekar, S. C.; Levitt, M. H. *J. Magn. Reson.* **1995**, *115*, 7–19. (b) Antzutkin, O. N. *Prog. NMR Spectrosc.* **1999**, *35*, 203–266.
(21) Bak, M.; Rasmussen, J. T.; Nielsen, N. C. *J. Magn. Reson.* **2000**, *147*, 296–330.
(22) Sheldrick, G. M.; Kruger, G. M.; Goddard, R. SHELXS-86, Structure Solution Program. *Acta Crystallogr., Sect. A: Found. Crystallogr.* **1990**, *A46*, 467–473.
(23) Sheldrick, G. M. *SHELXL-93, Program for Crystal Structure Refinement*; University of Gottingen: Gottingen, Germany, 1993, 1986; pp 63−119.
(24) Olivieri, A. C.; Frydman, L.; Grasseli, M.; Diaz, L. E. *Magn. Reson. Chem.* **1988**, *26*, 281–286.
(25) (a) Alla, M.; Lippmaa, E. *Chem. Phys. Lett.* **1976**, *37*, 260–264. (b) Opella, S. J.; Frey, M. H. *J. Am. Chem. Soc.* **1979**, *101*, 5854–5856. (c) Zilm, K. W. In *Spectral Editing Techniques: Hydrocarbon Solids, Encyclopedia of NMR*; Grant, D. M., Harris, R. K., Eds.; John Wiley & Sons Ltd.: Chichester, U.K., 1996; Vol. VII, pp 4498−4504.
(26) (a) Potrzebowski, M. J. *Eur. J. Org. Chem.* **2003**, *8*, 1367–1376. (b) Brown, S. P.; Spiess, H. W. *Chem. Rev.* **2001**, *101*, 4125–4155. (c) Frydman, L. *Annu. Rev. Phys. Chem.* **2001**, *52*, 463–498. (d) Tycko, R. *Annu. Rev. Phys. Chem.* **2001**, *52*, 575–606. (e) Bryce, D. L.; Bernard, G. M.; Gee, M.; Lumsden, M. D.; Eichele, K.; Wasylishen, R. E. *Can. J. Anal. Sci. Spectr.* **2001**, *46*, 46–82.
(27) (a) Harris, R. K. *Analyst* **2006**, *131*, 351–373. (b) Harris, R. K. *J. Pharm. Pharmacol.* **2007**, *59*, 225–239. (c) Harris, R. K.; Hodgkinson, P.; Pickard, C. J.; Yates, J. R.; Zorin, V. *Magn. Reson. Chem.* **2007**, *45*, S174–S186.
(28) Lyerla, J. R. In *Methods in High Resolution NMR Spectroscopy of Synthetic Polymers in Bulk* (*Stereochemical Analysis*); Komoroski, R. A., Ed.; VCH: Deerfield Beach, FL, 1986; Vol. 7, p 63.
(29) Kołodziejski, W.; Klinowski, J. *Chem. Rev.* **2002**, *102*, 613–628.
(30) Fulber, C.; Demco, D. E.; Blumich, B. *Solid State Nucl. Magn. Reson.* **1996**, *6*, 213–223.
(31) (a) Hu, J.; Wang, W.; Liu, F.; Solum, M. S.; Alderman, D. W.; Pugmire, R. J. *J. Magn. Reson., Ser. A* **1995**, *113*, 210–222. (b) Alderman, D. W.; McGeorge, G.; Hu, J. Z.; Pugmire, R. J.; Grant, D. M. *Mol. Phys.* **1998**, *95*, 1113–1126. (c) Frydman, L.; Chingas, G. C.; Lee, Y. K.; Grandinetti, P. J.; Eastman, M. A.; Barral, G. A.; Pines, A. *J. Chem. Phys.* **1992**, *97*, 4800–4808. (d) Kolbert, A. C.; Griffin, R. G. *Chem. Phys. Lett.* **1990**, *166*, 87–91.
(32) Dixon, W. T. *J. Chem. Phys.* **1982**, *77*, 1800–1809.
(33) Gu, Z. T.; McDermott, A. *J. Am. Chem. Soc.* **1993**, *115*, 4282–4285.
(34) Gu, Z. T.; Zabrano, R.; McDermott, A. *J. Am. Chem. Soc.* **1994**, *116*, 6368–6372.
(35) Ando, I.; Kuroki, S.; Kurosu, H.; Yamanobe, T. *Prog. Nucl. Magn. Reson. Spectrosc.* 2001, *39*, 79−133, and references cited therein.
(36) (a) Oldfield, E. *Annu. Rev. Phys. Chem.* 2002, *53*, 349−378, and references cited therein; (b) Wei, Y.; Lee, D. K.; Ramamoorthy, A. *J. Am. Chem. Soc.* **2001**, *123*, 6118–6126.
(37) Ye, C.; Fu, R.; Hu, J.; Hou, L.; Ding, S. *Magn. Reson. Chem.* **1993**, *31*, 699–704.